



ELSEVIER

Available online at www.sciencedirect.com

SCIENCE @ DIRECT®

Physica A 318 (2003) 307–318

PHYSICA A

www.elsevier.com/locate/physa

Scaling of cluster mass between two lines in 3d percolation

Luciano R. da Silva^{a,b,*}, Gerald Paul^a, Shlomo Havlin^{a,c},
Don R. Baker^{a,d}, H. Eugene Stanley^a

^aCenter for Polymer Studies and Department of Physics, Boston University, Boston, MA 02215, USA

^bDepartamento de Física, UFRN, 59072-970 Natal, RN, Brazil

^cDepartment of Physics, Bar-Ilan University, Ramat-Gan, Israel

^dDepartment of Earth and Planetary Sciences, McGill University, 3450 rue University, Montréal, Canada QC H3A 2A7

Received 1 August 2002

Abstract

We consider the cluster mass distribution between two lines of arbitrary orientations and lengths in porous media in three dimensions, and model the porous media by bond percolation at the percolation threshold p_c . We observe that for many geometrical configurations the mass probability distribution presents power law behavior. We determine how the characteristic mass of the distribution scales with such geometrical parameters as the line length, w , the minimal distance between lines, r , and the angle between the lines, θ . The fractal dimensions of the cluster mass are independent of w, r , and θ . The slope of the power-law regime of the cluster mass is unaffected by changes in these three variables; however the characteristic mass of the cluster depends upon θ . We propose new scaling functions that reproduce the θ dependence of the characteristic mass found in the simulations.

© 2002 Published by Elsevier Science B.V.

1. Introduction

Percolation theory is one of the best ways to investigate the structure of disordered media, particularly porous media [1–4]. Here we use percolation theory to analyze the mass distributions of clusters that are connected in configurations of the type shown in Fig. 1, configurations in which the two lines are connected by occupied bonds. The *cluster mass* is the number of bonds that are connected to the two lines (Fig. 1(a)). The *backbone* of the cluster is the set of bonds that are connected to the two lines through

* Corresponding author.

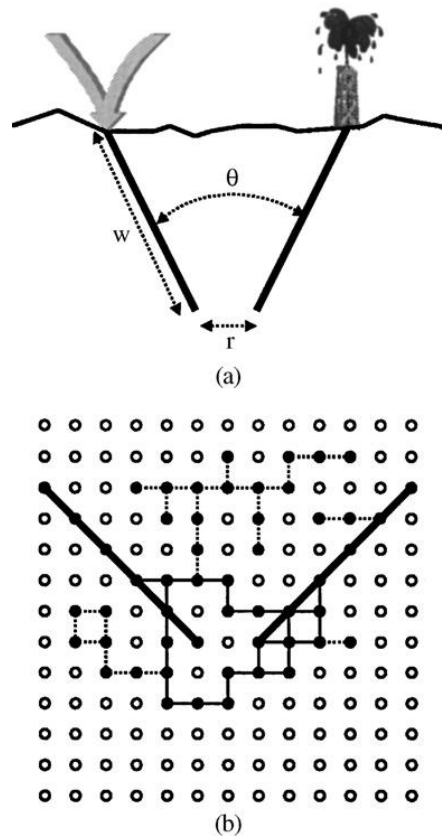


Fig. 1. (a) Illustration of well geometry. (b) Examples of a percolation cluster with two line wells with parameters $r = 2$, $\theta = 90^\circ$, and $w = \sqrt{50}$. The filled sites are members of the percolation cluster, which has a mass of 52. Solid lines form the backbone, which has a mass of 28.

independent paths (i.e., paths that have no common bond [5–8]). For configurations of two points, the distributions of various quantities have been studied [9–15]. Recently the distribution of the shortest paths between two lines for a three-dimensional cubic lattice [13] has been studied. Here we calculate the cluster mass distributions as a complement to our earlier study of the backbone mass distribution of the same clusters [16].

This study is motivated by the application of percolation theory to the techniques of oil recovery [17]. A commonly used technique in oil recovery is the injection of fluid into the ground at one site in the field in order to force oil out of the ground at another site nearby (Fig. 1). It is common to inject the fluid along a portion of the length of the injection well and to collect the oil along a portion of the length of the production well (as opposed to injecting and collecting at single points on the wells). In our model, each line represents a well in the oil field. One line represents the injection well, and the other the production well. In many cases the oil reservoir is extremely heterogeneous, and the percolation model is appropriate. Separation of oil reservoir rocks into two types—high permeability and low or zero permeability—can be modeled in percolation simulations, with the high-permeability rock represented by

occupied bonds and the low-permeability rock represented by unoccupied bonds. The connected mass represents the total oil in the reservoir connected to the two wells and the backbone mass the recoverable oil. Of course this model is only a crude approximation of a real oil field. Actual oil fields have strong correlations due to layering in the rocks, preferential orientation of porosity, etc. Viscous forces also play an important role during oil migration, which these models do not consider. Furthermore, actual oil fields are rarely at the percolation threshold. Nevertheless, this work provides important insights into how well geometry may affect the percolation cluster mass.

2. Simulations

We perform a numerical study of the system using Monte-Carlo simulations. We specify two sets of points representing lines in a simple cubic lattice to be the wells and we grow the cluster from these two lines of seeds. If the growth of either cluster stops before the two clusters connect, we discard the realization. For realizations in which the two clusters connect, the simulation ends either when the cluster growth stops naturally, or when the cluster mass reaches some specified limit, which is imposed to constrain the use of cpu time. To eliminate finite size effects, we use the technique of Ref. [18] to simulate systems on lattices of large enough size that the clusters never reach the edge of the lattice. We perform the simulations at the percolation threshold, $p_c = 0.2488126$ [19]. The configurations are characterized by three parameters: length w , angle θ , and minimal distance r (see Fig. 1(a)). We treat configurations in which the two wells are co-planar. Ref. [18] examines the distributions of shortest paths between non-coplanar wells and finds that the asymptotic behavior of the distributions is independent of whether the wells are coplanar or not. For each configuration, we run at least 10^6 non-discarded realizations. We calculate the cluster mass for each of the simulations as exemplified in Fig. 1(b).

3. General observations

We expect to find an initial cutoff in the cluster mass distributions due to the fact that these masses cannot be smaller than the distance τ . Somewhere above this minimum cutoff we expect to observe a regime that exhibits power-law behavior. These general features of the distributions have been observed in the distributions for other quantities [9–13]. The quantities of interest are (i) the most-probable value of the distribution (the maximum), the scaling of which will be determined by the fractal dimensions of the quantities measured, and (ii) the slope of the power-law regime. For clusters grown from a single point, the slopes of the power-law regimes of the cluster distributions are $\tau - 1$, where τ is the Fisher exponent. The fractal dimensions and power-law regime slopes are related by [1,3,5]

$$\tau - 1 = \frac{d}{d_f}, \quad (1)$$

where d is the dimension of the system, and d_f is the fractal dimension of the cluster. For $d = 3$, estimates for these values are [20,21]

$$d_f = 2.524 \pm 0.008, \quad (2)$$

$$\tau - 1 = 1.189 \pm 0.004. \quad (3)$$

4. Cluster mass

4.1. Parallel wells

In order to gain insight into the general behavior, we first study parallel wells ($\theta=0$) see Fig. 2(a). We consider first the following limiting cases:

- (i) $w \ll r$ —In this case, we approximate the configuration by two points (see Fig. 2(b)). In Fig. 3(a) we show the mass probability distribution $P(m|r)$ for $w = 0$ and $r = 1, 2, 4, 8, 16, 32$ and 64 . The distribution shows a maximum followed by a power-law regime with slope -1.18 , consistent with Eq. (3). We study also how the characteristic mass m^* , corresponding to peak of the distribution, scales with the distance r . The log–log plot of m^* vs. r in Fig. 3b indicates that m^* scales with exponent $d_B \cong 2.6$ which is consistent with Eq. (2).
- (ii) $w \gg r$ —For this case (see Fig. 2(c)) we approximate the configurations by $r = 0$ (a single line). We perform the same analysis as before, and obtain similar results (see Fig. 4(a)) i.e., power-law distribution for $P(m|w)$ with a slope ≈ -1.18 and fractal dimension ≈ 2.55 (Fig. 4(b) and (c)).

We now study cases intermediate to those studied in (i) and (ii). In Fig. 5a, we plot the distribution of cluster mass for configurations in which $r = 16$ and we vary w from 0 to 64. For small w , the distributions are essentially unchanged, but for to $w \gg r$, the distributions scale with the exponent d_f (Fig. 5a and b).

We now develop a scaling form for the dependence of the characteristic mass m^* on r and L , the system size. Without loss of generality we can write

$$m^*(r, L) = \left[f \left(\frac{r}{w} \right) r \right]^{d_f}. \quad (4)$$

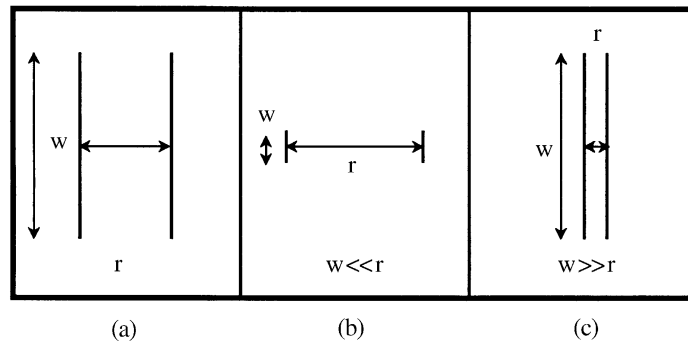


Fig. 2. Parallel well examples. (a) General case. (b) $w \ll r$. (c) $w \gg r$.

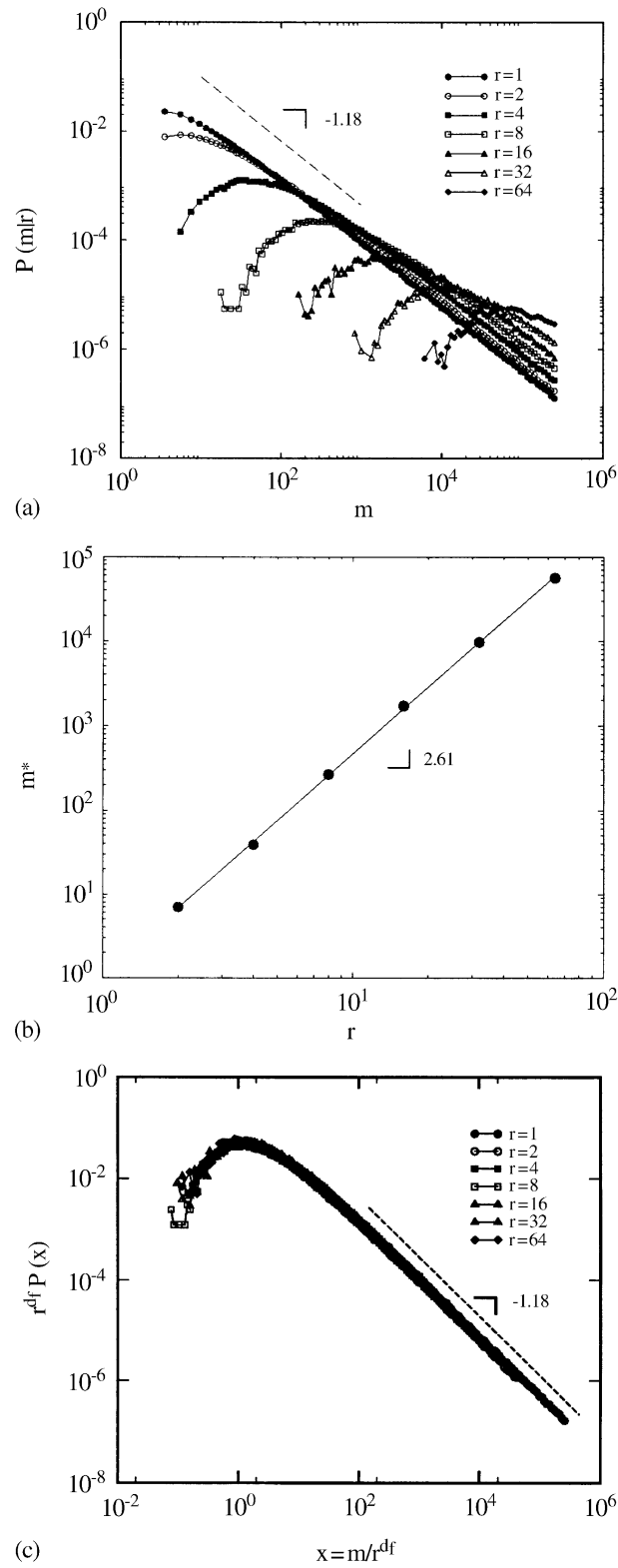


Fig. 3. (a) Cluster mass distribution $P(m|r)$, for the percolation cluster for the two points case ($w = 0$), for several values of r ($r = 1, 2, 4, 8, 16, 32, 64$). The line of slope -1.18 denotes the theoretical expectation. (b) Scaling behavior of m^* , the most probable mass, as a function of r . The fitted slope of 2.61 is consistent with the fractal dimension $d_f = 2.54$. (c) Plots of (a) collapsed using $d_f = 2.61$.

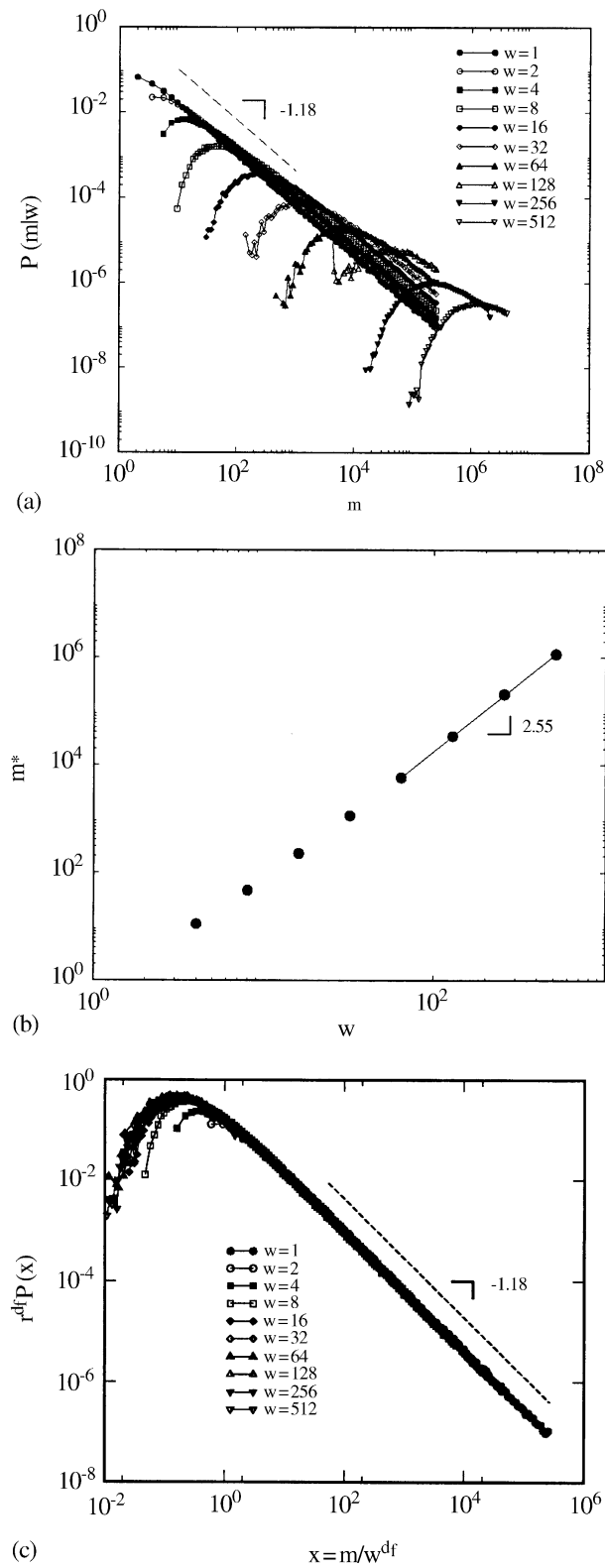


Fig. 4. (a) Cluster mass distribution $P(m|w)$ for ($r=0$) for several values of w ($w = 1, 2, 4, 8, 16, 32, 64, 128, 256, 512$). (b) Scaling behavior of m^* as a function of w . (c) Plots of (a) collapsed using $d_f = 2.55$.

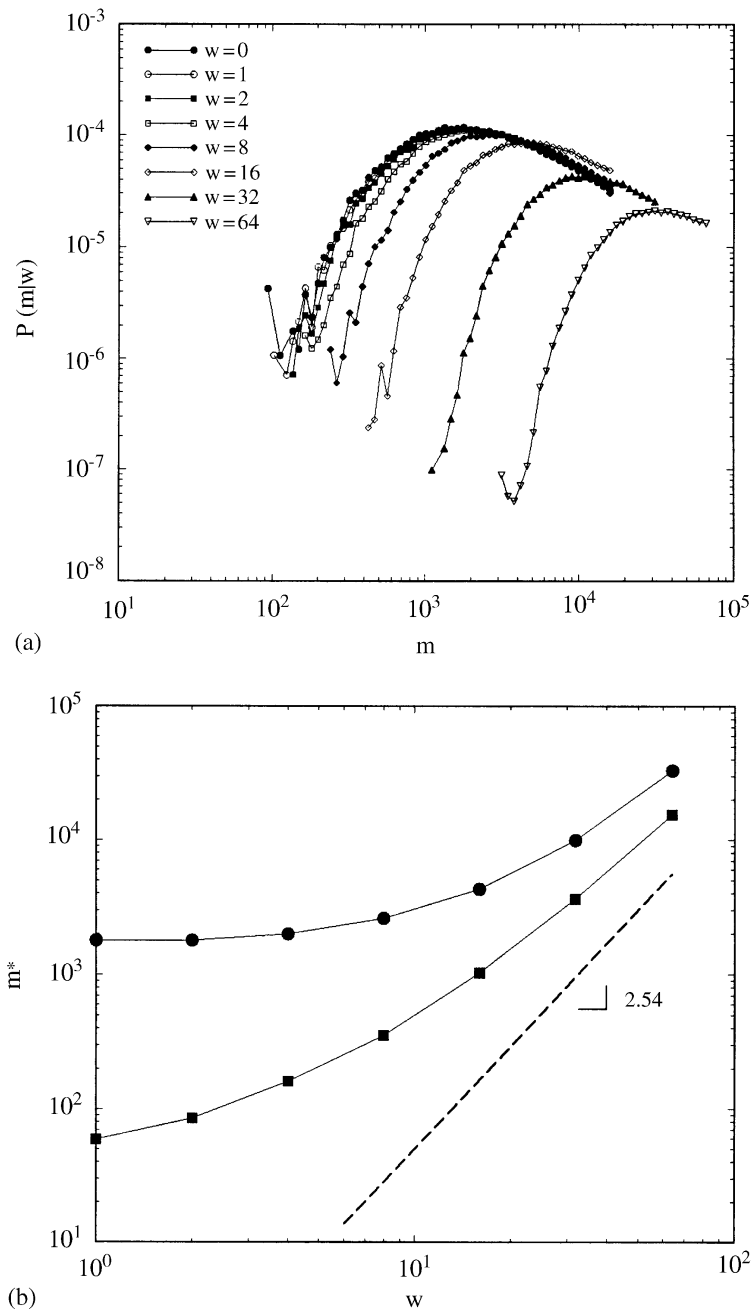


Fig. 5. (a) Mass distribution $P(m|w)$ for two parallel wells with $r = 16$ and $w = 0, 1, 2, 4, 8, 16, 32, 64$. (b) Scaling behavior of m^* versus w for $r = 4$ (circles) and for $r = 16$ (squares).

This form is consistent with the scaling of the cluster mass (Figs. 3(c) and 4(c)). That is, if

$$\begin{aligned}
 r' &\equiv \alpha r, \\
 w' &\equiv \alpha w,
 \end{aligned}
 \tag{5}$$

then

$$m^*(r', L') = \left[f\left(\frac{r'}{w'}\right) r' \right]^{d_f} = \left[f\left(\frac{r}{w}\right) \alpha r \right]^{d_f} = \alpha^{d_f} m^*(r, L). \quad (6)$$

Having confirmed above that the numerical results of our obey scaling, $m^*(r, L)$ can be written as,

$$m^*(r, L) = \left[ar + g\left(\frac{r}{w}\right) w \right]^{d_f}, \quad (7)$$

since w and r become irrelevant variables for $r \gg w$ and $r \ll w$, respectively. Thus we expect

$$g\left(\frac{r}{w}\right) \rightarrow \begin{cases} 0 & r \gg w, \\ \text{constant} & r \ll w. \end{cases} \quad (8)$$

4.2. Non-parallel wells

We now study non-parallel wells. The results for the mass probability distribution $P(m|\theta)$ are shown in Fig. 6(a). We find that the power-law regime is consistent with a slope -1.18 independent of θ . We consider also the peak of these distributions, analyzing how m^* evolves with θ . Fig. 6(b) shows the dependence of m^* vs. θ . m^* increases rapidly for small values of θ , and for larger θ asymptotically approaches a limiting value at, $\theta = \pi$.

We now suggest a functional form for the dependence of the characteristic mass m^* on θ . Without loss of generality we can write

$$m^*(\theta) = m^*(0)[f(\theta)]^{d_f}. \quad (9)$$

Since the configuration for $\theta = \pi$ is simply a single straight line twice the length of the single line for $\theta = 0$, we expect

$$m^*(\pi) = m^*(0)2^{d_f}. \quad (10)$$

We then are motivated to write

$$m^*(\theta) = m^*(0)[1 + g(\theta)]^{d_f}, \quad (11)$$

where $g(\theta)$ is monotonic and

$$g(0) = 0$$

and

$$g(\pi) = 1.$$

A first guess at a functional form for $g(\theta)$ is some power of $\sin(\theta/2)$ but no power seems to fit the data of Fig. 6(b) well. A functional form that fits better is

$$h(\theta) = \sin \left[\frac{\pi}{2} \sin \left(\frac{\theta}{2} \right) \right]^{0.4}. \quad (12)$$

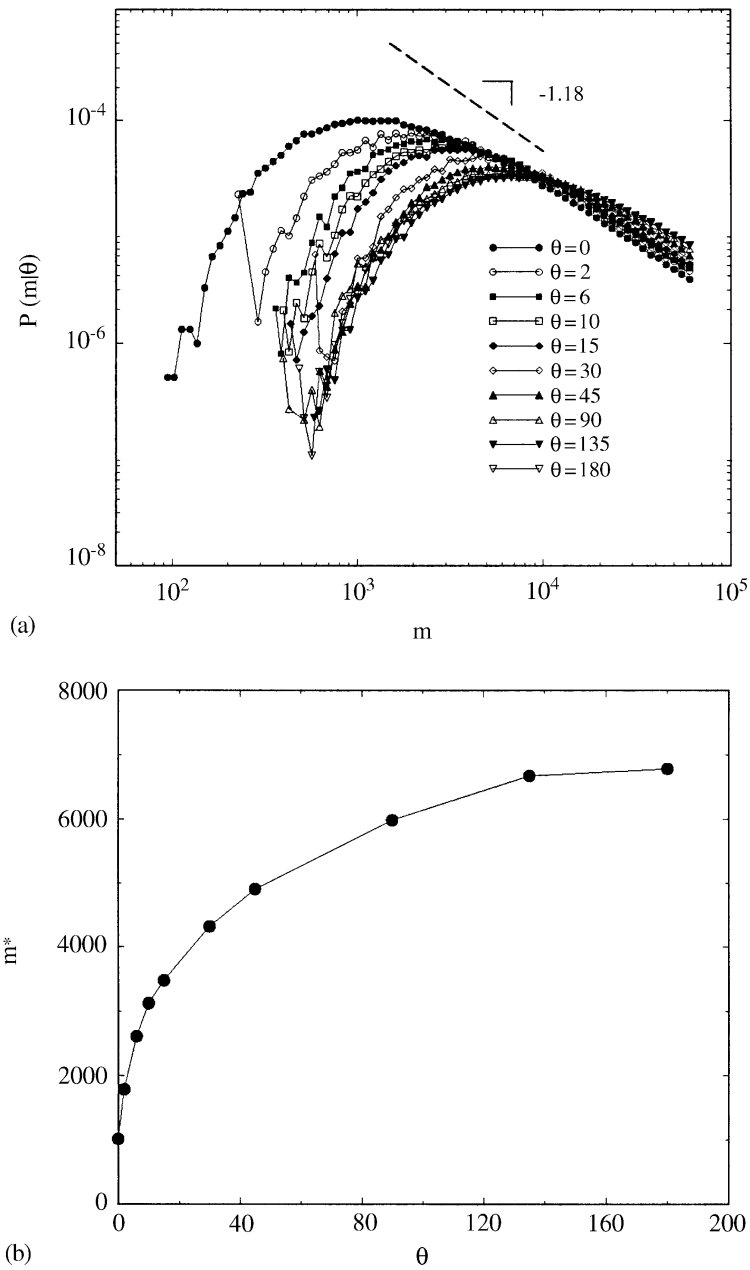


Fig. 6. (a) Mass distribution $P(m|\theta)$ for $r = 0$ and $w = 32$ for the percolation cluster to the general non parallel wells for several values of the angle θ . (b) Corresponding scaling behavior of m^* versus θ .

The final functional form for $m^*(\theta)$ is thus

$$m^*(\theta) = m^*(0) \left(1 + \sin \left[\frac{\pi}{2} \sin \left(\frac{\theta}{2} \right) \right] \right)^{0.4 d_f}, \tag{13}$$

where the exponent 0.4 is obtained by the power law fit in Fig. 7(a). We note that there is no a priori justification for this form; it simply satisfies the appropriate boundary

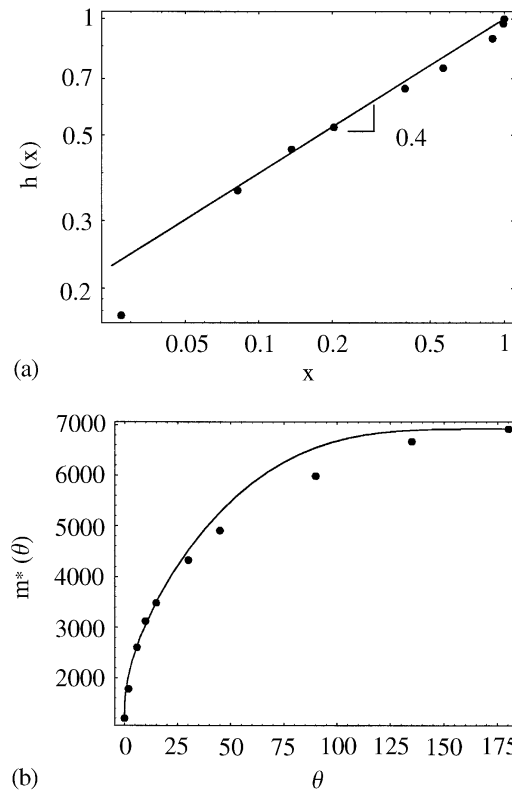


Fig. 7. (a) Determination of exponent in Eq. (11), where $x \equiv \sin[(\pi/2) \sin(\theta/2)]$. (b) Comparison of functional form $m(\theta)$ (solid line) versus observed data.

conditions and fits the simulation results reasonably well, as shown in Fig. 7(b). This simple expression relating cluster mass with the angle of the two lines provides important information for the orientation of wells designed to intersect the largest possibly cluster mass from which they might extract oil.

5. Discussion

We have analyzed the distributions of cluster mass for various configurations of 2-line $3d$ percolation clusters. The cluster mass distributions are independent of the angle θ between the lines, in contrast to the dependence of the power-law regime exponent of the cluster backbone mass distribution [16] and the power-law regime exponent of the shortest path between two lines [13]. Our experimental discovery that the power-law regime exponent for some quantities is dependent on θ and for other quantities is independent of θ is still not understood.

The dependence of the power-law regime exponent of the cluster mass distribution in restricted spaces-wedges of angle θ -has been predicted by Cardy for $2d$ using conformal invariance arguments [22]. These configurations are different from the configurations we study here in which the space is not restricted; rather we investigate clusters between

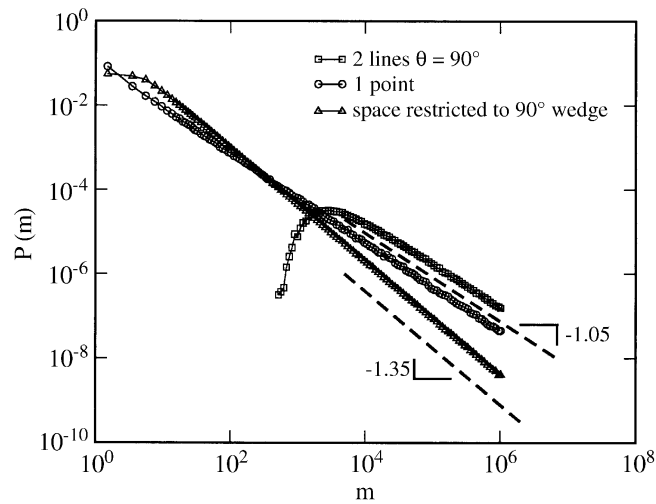


Fig. 8. Cluster mass distribution $P(m)$ in 2 dimensions for clusters starting from one point, clusters connecting two lines with $\theta=90^\circ$, $w=32$ and $r=0$, and clusters growing in a wedge bounded by two lines intersecting at an angle of 90° . The power-law exponents for clusters starting at a point and connecting two lines are the same, whereas the power-law exponent for clusters growing in restricted space is significantly larger.

two lines oriented at angle θ . In order to confirm the difference of these configurations we have performed $2d$ simulations, the results of which are plotted in Fig. 8. Three simulations were performed in $2d$ at the percolation threshold using the techniques discussed above. In the first simulation, clusters were grown from a single point in space. In the second simulation, clusters were grown between two lines with $r=0$, $w=32$ and $\theta=90^\circ$ in space. As found in $3d$, the slopes of the power-law regime of the distribution of cluster size in these two simulations are the same. The slopes of both power-law regimes for these two simulations shown in Fig. 8 are ≈ 1.05 , consistent with the $2d$ value of $\tau - 1 = \frac{96}{91}$ [1]. In the third simulation, designed to reproduce the geometry of Cardy's calculation [22], the clusters were grown in space restricted to a 90° wedge; for this case the power-law exponent of the cluster mass is 1.35, see Fig. 8. These results demonstrate that our configurations are different from those of Cardy—our lines oriented at $\theta=90^\circ$ to each other are embedded in space and the cluster can grow past them, whereas the lines in Ref. [22] form two boundaries of space and clusters cannot cross them. Thus, the results of [22] do not presently provide insight into the percolation behavior discovered in this study; however other applications of conformal invariance theory may possibly provide the key to understanding the θ dependence of the exponents observed in this paper.

Acknowledgements

We thank L. Braunstein, S.V. Buldyrev, Andre Moreira for helpful discussions, and British Petroleum, CTPETRO/Cenpes/Petrobras, CPNq, the National Science Foundation and NSERC for support.

References

- [1] A. Bunde, S. Havlin (Eds.), *Fractal and Disordered Systems*, 2nd Edition, Springer, Berlin, 1996, and references therein.
- [2] D. Ben-Avraham, S. Havlin, *Diffusion and Reactions in Fractals and Disordered Systems*, Cambridge University Press, Cambridge, 2000.
- [3] D. Stauffer, A. Aharony, *Introduction to Percolation Theory*, Taylor and Francis, London, 1992.
- [4] M. Sahimi, *Applications to Percolation Theory*, Taylor and Francis, London, 1992.
- [5] H.J. Herrmann, H.E. Stanley, *Phys. Rev. Lett.* 53 (1984) 1121.
- [6] H.E. Stanley, *J. Phys. A: Math. Gen.* 10 (1977) L211.
- [7] A. Coniglio, *Phys. Rev. Lett.* 46 (1981) 250.
- [8] S. Havlin, P. Ben-Avraham, *Adv. Phys.* 36 (1987) 695.
- [9] N.V. Dokholyan, Y. Lee, S.V. Buldyrev, S. Havlin, P.R. King, H.E. Stanley, *J. Stat. Phys.* 93 (1998) 603.
- [10] Y. Lee, J.S. Andrade Jr., S.V. Buldyrev, S. Havlin, P.R. King, G. Paul, H.E. Stanley, *Phys. Rev. E* 60 (1999) 3425.
- [11] J.S. Andrade Jr., S.V. Buldyrev, N. Dokholyan, P.R. King, Y. Lee, S. Havlin, H.E. Stanley, *Phys. Rev. E* 62 (2000) 8270.
- [12] M. Barthélémy, S.V. Buldyrev, S. Havlin, H.E. Stanley, *Scaling for the critical percolation backbone*, *Phys. Rev. E* 60 (1999) R1123.
- [13] G. Paul, S. Havlin, H.E. Stanley, *Phys. Rev. E* 65 (2002) 066105.
- [14] P. Grassberger, *J. Phys. A: Math. Gen.* 32 (1999) 6233.
- [15] R.M. Ziff, *J. Phys. A* 32 (1999) L457.
- [16] L.R. da Silva, G. Paul, S. Havlin, D.R. Baker, H.E. Stanley, *Physica A* 314 (2002) 140.
- [17] P.R. King, in: A.T. Buller, et al. (Eds.), *North Sea Oil and Gas Reservoirs*, Vol. II, Graham and Trotman, London, 1990.
- [18] G. Paul, R.M. Ziff, H.E. Stanley, *Phys. Rev. E* 64 (2001) 026115.
- [19] C.D. Lorenz, R.M. Ziff, *Phys. Rev. E* 57 (1998) 230.
- [20] R.M. Ziff, G. Stell, P.N. Strenski, R.M. Bradley, J.M. Debierre, *Phys. Rev. Lett.* 66 (1991) 133.
- [21] M.D. Rintoul, H. Nakanishi, *J. Phys. A* 27 (1994) 5445.
- [22] J.L. Cardy, *Nucl. Phys. B* 240 (1984) 514.